Journal of Drug Delivery Science and Technology 55 (2020) 101481

Contents lists available at ScienceDirect

Journal of Drug Delivery Science and Technology

journal homepage: www.elsevier.com/locate/jddst

Folic acid mediated endocytosis enhanced by modified multi stimuli nanocontainers for cancer targeting and treatment: Synthesis, characterization, in-vitro and in-vivo evaluation of therapeutic efficacy

E.K. Efthimiadou[a,e,*], P. Lelovas[d], E. Fragogeorgi[b,c], N. Boukos[a], V. Balafas[d], G. Loudos[b,c], N. Kostomitsopoulos[d], M. Theodosiou[a], A.L Tziveleka[a], G. Kordas[a]

[a] Institute for Nanoscience and Nanotechnology, NCSR "Demokritos", 153 10, Aghia Paraskevi Attikis, Greece
[b] Radiochemical/ Radiopharmacological Quality Control Laboratory, Institute of Nuclear and Radiological Sciences and Technology, Energy & Safety, N.C.S.R. 'Demokritos', 15310, Aghia Paraskevi, Greece
[c] Department of Medical Instruments Technology, Technological Educational Institute, GR 122 10, Athens, Greece
[d] Clinical, Experimental Surgery, & Translational Research, Biomedical Research Foundation Academy of Athens (BRFAA), Athens, 11527, Greece
[e] Inorganic Chemistry Laboratory, Department of Chemistry, National and Kapodistrian University of Athens, Greece

ARTICLE INFO

Keywords:
Targeted delivery
Multi sensitive
Nanocontainers
Endocytosis

ABSTRACT

Polymeric materials are in the epicenter of scientific research the last decade and have been used in a range of pharmaceutical and biological applications. Multifunctional polymeric materials are capable targeting agents, which can be used as controlled drug release vehicles for the enhancement of therapeutic efficacy, as well as for diagnostic purposes. A newer generation of these smart polymeric entities constitutes of smart nanocontainers (NCs), which can navigate the drug to specific areas by avoiding random distribution, and thus resulting in drug toxicity reduction. The combination of pH, thermo and redox sensitivity of the multi stimuli NCs can help to achieve specific release of the drug in the tumor area, where these sensitivity parameters can be observed. Hollow polymeric multi stimuli fluorescent tNCs based on N-(2-Hydroxypropyl)methacrylamide (HPMA) were successfully functionalized with a specific targeting moiety; folic acid, and then characterized morphologically, by scanning electron and transmission electron microscopy, as well as structurally, by Fourier-transform infrared spectroscopy. Their targeting mechanism was investigated *in vitro* in cervical cancer cell lines and *in vivo* in tumor bearing mice. According to our results the folic acid functionalized NCs targeted HeLa cells' surface within the first 30 min of treatment. Human tumor xenografted mice (nonobese diabetic/severe combined immunodeficient) were injected with folate functionalized NCs and their tumor uptake was estimated by γ-imaging at about 3.5%. The targeting efficiency of the folate functionalized NCs was investigated directly *in vivo* by γ-imaging and indirectly by a tumor efficacy protocol.

1. Introduction

Notably nanometer sized polymeric drug carriers including dendrimers, polymeric micelles, liposomes and recently hollow polymeric nanocontainers (NCs) have been widely investigated as drug delivery systems aiming to confront a variety of cancer types [1–14]. These nanocarriers present many advantages such as better circulation time, enhanced permeability and retention time, and especially reduced toxicity. Many research groups focus on effectively coating these systems with polyethylene glycol (i.e., PEGylated) [15], poly lactic acid (PLA) [13] or inert thermo/pH responsive polymers such as acrylates [16,17] and N-(2-Hydroxypropyl)methacrylamide (HPMA) copolymers which can improve stealth properties and selective responses [13,15]. HPMA copolymers have been widely used as polymeric delivery systems to modify the biodistribution of toxic drugs [18–20]. They also benefit from passive tumor accumulation through the enhanced permeability and retention effect (EPR), which is when macromolecules extravasate into tumor tissue through discontinuous blood vessels and remain there due to impaired lymphatic drainage [15,18–22]. However, HPMA is broadly used in the field of linear or grafted copolymers there is no previous reported work about the fabrication NCs [18–20]. Based on previous investigations drugs attached to HPMA demonstrate increased stability and *in vitro* activity [21]. Additionally, introducing tumor targeting groups into micro/nano-sphere's surface it can further

* Corresponding author. Institute for Nanoscience and Nanotechnology, NCSR "Demokritos", 153 10, Aghia Paraskevi Attikis, Greece.
E-mail addresses: e.efthimiadou@inn.demokritos.gr, efthim@chem.uoa.gr (E.K. Efthimiadou).

https://doi.org/10.1016/j.jddst.2019.101481
Received 17 July 2019; Received in revised form 19 December 2019; Accepted 26 December 2019
Available online 07 January 2020
1773-2247/ © 2020 Elsevier B.V. All rights reserved.

enhance their accumulation in cancer cells via active targeting [1,2,10,21,23–28]. This kind of functionalization improves the biodistribution of the carried drugs and significantly enhances the nanosystem's therapeutic index while minimizing side effects. Many first-line anticancer drugs, such as doxorubicin, taxotere and platinum-based drugs present various side effects, some of which are considerably severe [29–33]. The encapsulation of these drugs into functionalized systems improves the drug's metabolism, biodistribution and circulation time [26,27,34–37]. In this concept and in the frame of the present study, we have introduced both a targeting agent; folate [1], and a thermosensitive agent; iron oxide magnetic nanoparticles, in order to combine a targeted cancer therapy whilst enhancing drug release through magnetic hyperthermia [12,38–40]. Generally, the exposure of superparamagnetic nanoparticles to an alternating magnetic field, results in heat generation. It is reported that direct injection of magnetic nanoparticles into solid tumors and the sequential exposure to an alternating magnetic field is capable of inducing tumor regression due to hyperthermic susceptibility of cancer cells [41]. Specifically, we developed hybrid nanocontainers with a variety of interesting properties and perspectives, including instant dispensability, pH, thermo and redox reversible behavior, and novel magneto-responsive properties [11,16,42–45].

In this work we have synthesized and characterized Yolk-type [45,46] core-shell NCs as novel drug delivery systems. HPMA was synthesized through methacryloyl addition to aminopropan-2-ol and the resultant product was characterized by nuclear magnetic resonance (NMR). The Yolk-Type NCs were synthesized via seed emulsion polymerization and then characterized structurally and morphologically. The isolated NCs were further chemically modified, first with magnetic nanoparticles through deposition and then with the folate moiety and/or fluorescein through carbodiimide chemistry (Scheme 1). This resulted in simultaneous optimization of their magnetic hyperthermia efficacy and their targeting properties. These multi targeting hollow NCs (tNCs) were loaded with the anticancer drug doxorubicin (DOX) and their release properties were investigated under different pH, thermo- and redox conditions. Their targeting mechanism was investigated *in vitro* in Human epithelial cervical cell line (HeLa), which overexpresses the folate receptor (FR) and in Human Caucasian breast adenocarcinoma cell line (MCF-7) which do not express the FR. In order to investigate the *in vivo* targeting ability of tNCs, xenografted nonobese diabetic/severe combined immunodeficient (NOD/SCID) mice, were subjected to γ-imaging for tumor uptake. Therapeutic efficacy of tNCs loaded with DOX was studied in another protocol using xenografted NOD/SCID mice with HeLa cells.

2. Experimental

2.1. Materials & methods

Methyl Methacrylate (MMA), which was purchased from Merck, was freshly distilled before its use and Potassium persulfate (KPS) was purchased from Panreac and used as received. Divinyl Benzene (DVB) and Poly(ethylene glycol) methacrylate (average Mn = 360) (PEG-360) were also purchased from Aldrich and used as received. Ethylene Glycol (EG) provided by Merck, Iron (II) Chloride tetrahydrate ($FeCl_2 \times 4H_2O$) provided by Riedel-de Haën, Potassium Nitrate (KNO_3) provided by Acros, Hexamethylenetetramine (HETM) provided by Alfa Aesar and 95° commercial ethanol were used as received. N,N'-(disulfanediylbis (ethane-2,1-diyl))bis(2-methylacrylamide) (Disulfide) and N-(2-Hydroxypropyl) methacrylamide (HPMA) were synthesized and characterized in our lab (See paragraph 2.3). Methacryloyl chloride (97%) was purchased from Alpha Aesar and freshly distilled before its use. Dimethyl formamide (DMF), Dymethyl sulfoxide (DMSO) and N,N′-Diisopropylcarbodiimide (DIC) were purchased from Sigma-Aldrich. The 1-Aminopropan-2-ol, was obtained from Alpha Aesar and was used without purification. $CDCl_3$ (> 99.8%) stabilized over a silver coil was purchased from Euriso-top. LysoTracker Red was purchased from Lonza, Walkersville, MD. Deionized water was used for all polymerization procedures.

Doxorubicin·HCl (DOX) was provided by Pharmacia & Upjohn and used as received. High glucose Dulbecco's modified Eagle Medium (DMEM) and MTT were purchased from Sigma. Trypsin-EDTA, L-glutamine, penicillin–streptomycin solution and heat inactivated fetal bovine serum (FBS) were obtained from Biochrom KG. Technetium-99 m was used as a $Na^{99m}TcO_4$ solution in saline, eluted from a commercial Mallinckrodt Medical B.V. ^{99}Mo-^{99m}Tc generator.

2.2. Equipment

Scanning electron microscopy (SEM) and Transmission Electron Microscopy (TEM), images were obtained on an FEI Inspect microscope operating at 25 kV and a FEI CM20 microscope operating at 200 kV, equipped with a Gatan GIF200 Energy Filter utilized for EF-TEM elemental mapping, respectively. Fourier transform infrared (FT-IR) spectra were obtained with a PerkinElmer Spectrum 100 Spectrometer; the spectra were scanned over the range 4000–400 cm^{-1}. Nuclear Magnetic Resonance (NMR) spectra were obtained with a Bruker Advance DRX-500 instrument at 500 MHz. X-Ray Diffraction data were obtained with a powder diffractometer (SIEMENS D-500 equipped with a CuKa lamp with wavelength 1.5418 Å, Siemens AG). Dynamic light scattering (DLS) measurements were performed on a Malvern Instruments Zetasizer Nano Series, with a multipurpose titrator. In the data presented in this study, each measurement represents the average value of 3 measurements, with 11–15 runs for each measurement. UV–visible absorption spectra in the wavelength range of 200–800 nm were obtained on a Jasco V-650 spectrometer. An ultrasonic bath was used for sonication (Elma Sonic, S 30H). A Vibrating Sample Magnetometry (VSM) model 155 with a Bell 640 Gaussmeter, source: Danfysik System 8000 (−2 to 2 T) was used for the magnetic measurements. Magnetic fluid hyperthermia was performed by a 2.4 kW Easyheat 0224 system (Easyheat®, Ameritherm Inc) at a field strength of ~27 kA/m; for *ex vitro* experiments in solution in an 8 turn coil with 3.3 cm diameter operating at 270 kHz and for *in vivo* experiments in a 6-turn coil with 8.2 cm diameter operating at 163 kHz. Either coil was continuously water cooled. Temperature was recorded every second with an RF-immune fiber optic probe. Thermogravimetric analysis was performed via a TGA/DSC1 Mettler Toledo instrument under N_2 flow and the measurement was in temperature range of 25–800 °C at a step of 10 °C/min. A microplate reader Sirio S, SEAC Radim group (540/620 nm) was used to measure the optical density (O.D.) of the cell's suspension. Radioactivity of ITLC-SA strips and biodistribution samples were measured by a multi-sample gamma-counter, a Packard Minaxi 5500 equipped with a 3″ NaI (Tl) crystal. Scintigraphic imaging was performed using a custom high-resolution small animal gamma-camera with a 5 × 10 cm field of view. The system is based on: i) a parallel hole collimator, 25 mm t hick, with hexagonal holes 1.1 mm in diameter and 0.25 mm septa; ii) a 5 × 10 cm pixelized NaI scintillator, 5 mm thick, with 1 × 1 mm^2 pixels and 0.25 mm septa; iii) two square H8500 PSPMTs, each one 50 × 50 mm in size. The system has 1.5 mm spatial and 15% energy resolution (BioEmission Technology Solutions). Confocal BioRad, MRC 1024 ES was used for cell uptake studies.

2.3. Synthesis of N-(2-hydroxypropyl) methacrylamide (HPMA)

N-(2-Hydroxypropyl) methacrylamide (HPMA) was prepared by the reaction of 1-Aminopropan-2-ol with methacryloyl chloride (Scheme 1). 22.7 g (0.27 mol) of anhydrous sodium hydrogen carbonate was suspended in a solution of 20 g (0.27 mol) of 1-aminopropan-2-ol in 51 ml freshly distilled methylene chloride. The suspension was cooled to 0 °C and a solution of 21 g (0.27 mol) of methacryloyl chloride in 20 ml methylene chloride was added dropwise in 1 h period while temperature was kept at 0°C. The reaction mixture was stirred for

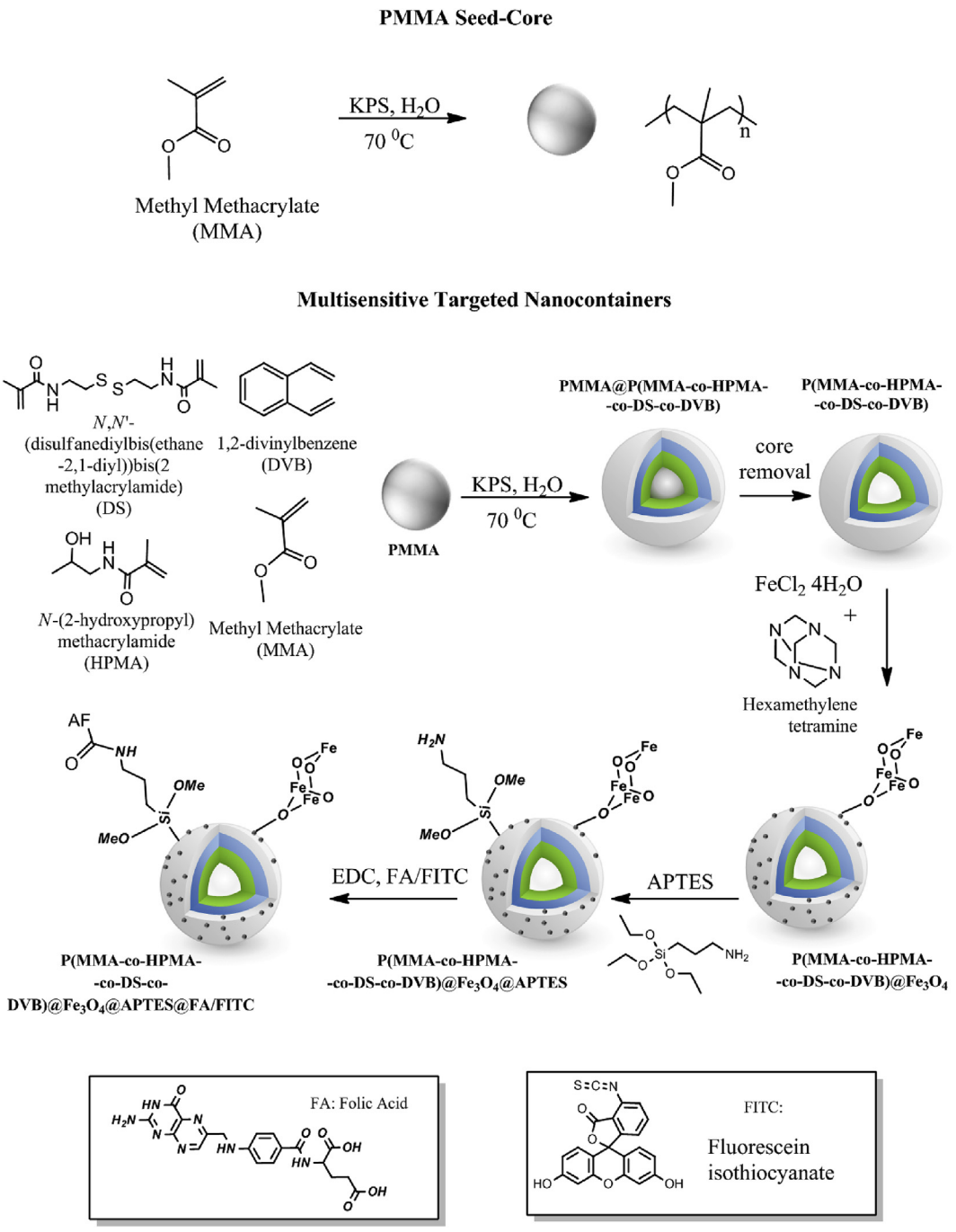

Scheme 1. Synthetic approach of PMMA@P(MMA-*co*-HPMA-*co*-DS-*co*-DVB)Fe_3O_4@APTES@Fitc@Folic Acid core-sell NCs.

another 2 h at 20 °C. Then 9.0 g of anhydrous sodium sulfate was added, the solid was filtrated and the filtrate solution was concentrated at one half of the initial volume. Then the HPMA was forced to precipitate by recrystallization from methylene chloride at −20 °C and was then washed by cool acetone. The product was purified by flash chromatography (9:1 EtOAC/Hexanes, Rf = 0.4) to give 10.6 g (73%) of an amorphous white solid. ^1H NMR (500 MHz, $CDCl_3$) δ 6.67(bs, 1H), 5.69 (d, 1H), 5.3 (d, 1H), 3.9 (m, 1H), 3.6 (m, 1H), 3.4 (m, 1H), 3.1 (m, 1H), 1.9 (s, 3H), 1.1 (s, 3H); ^{13}C NMR ($CDCl_3$) δ 156.78, 136.75, 128.85, 128.33, 79.78, 66.88, 65.78, 52.69, 40.57, 29.94, 28.64, 22.88.

2.4. Synthesis of N,N'-(disulfanediylbis(ethane-2,1-diyl))bis-(2-methyl acryl amide) (DS)

Cystamine dihydrochloride (3.0 g, 13.3 mmol, 1.0 eq) was added in aqueous solution and stirred for 30 min. The mixture was cooled at 5 °C and 4 equivalent of NaOH were added (2.08 g, 53.0 mmol, 4.0 eq). After 30 min of additional stirring, 2.0 equivalent of freshly distilled methacryloyl chloride (2.82 g, 27.0 mmol, 2.0 eq) were added dropwise via a dropping funnel. When the addition completed, the reaction was left to reach room temperature and then the mixture was left under stirring for additional 4 h. The desired product was isolated and purified according to the following procedure. The separated organic phase was extracted with dichloromethane (3 × 25 ml) and the collected solution was dried over Na_2SO_4. The mixture was filtered off and the

solvent was removed in vacuum. The resulted product (Fig. S1B), was purified by recrystallization from a 1:2 ethyl acetate/hexane mixture. Yield: 2.62 g, 98%). ^{1}H NMR ($CDCl_3$): 6.7 (sb, 2H, –NH), 5.72 (d, 2H, =CH, *cis*), 5.35 (d, 2H, =CH, *trans*), 3.61 (q, 4H, -NHCH_2), 2.85 (q, 4H, –SHCH_2), 1.96 (s, 6H, -CH_3). ^{13}C NMR ($CDCl_3$): 168.9 (C=O), 139.3 (C=C), 119.1 (C=C), 39.6 (-NHCH), 37(-SCH), 19.9 (-CH_3).

2.5. Synthesis of fitc/folic acid functionalized NCs (tNCs)

2.5.1. Synthesis of PMMA seed-core particles

In a typical emulsifier free radical polymerization, 1 ml of monomer MMA was added to 12 ml of distilled water in a 25 ml spherical flask. The flask was then placed under nitrogen over a magnetic stirrer and the temperature was increased to 80 °C. When temperature reached 80 °C and after 30 min of nitrogen supply, KPS is added (2% of the monomers). After 20 h of the polymerization, the resulted polymer was purified by centrifugation (3 times at 10000 rpm for 10 min).

2.5.2. Synthesis of PMMA@P(MMA-co-HPMA-co-DS-co-DVB) core-sell NCs

The PMMA@P(MMA-*co*-HPMA-*co*-DS-*co*-DVB) spheres were prepared by emulsion copolymerization of methyl methacrylate (MMA), N-Hydroxy propyl methylacrylamide (HPMA), and N,N'-(disulfanediylbis (ethane-2,1-diyl))bis-(2-methyl acryl amide) (DS). Divinyl benzene (DVB) served as a crosslinker. According to our procedure, 0.3 g of seeds were dispersed in a solution of water/ethanol (25:2) and in the dispersant 60 mg of HPMA, 640 μl of MMA and 300 μl of crosslinker DVB 45 μl and 60 mg of DS were added; the mixture was left under stirring for 2 h. Following, the spherical vial was covered by a septum and the solution was stirred for additional 30 min under nitrogen. Finally, 30 mg of KPS (2% w/w of monomers) was used as the initiator in order for the polymerization to start. The reaction proceeded for 12 h at 70 °C. The resulting product was washed by three cycles of centrifugation with deionized water and then the solid was dried at the vacuum. Hollow microspheres are prepared during the multi shell production due to Oswald mechanism. The cavity is created due to the migration of the seed polymer, towards the polymer surface as the polymerization proceeds, as supported in our previous work [47,48].

2.5.3. Synthesis of PMMA@P(MMA-co-HPMA-co-DS-co-DVB)@Fe_3O_4 core-shell NCs

The isolated hollow NCs (100 mg) were dispersed in a solution consisting of ethylenoglycol (EG) and water (EG/H_2O = 65/35 ml). The mixture remained for 1 h under nitrogen, while stirring, and then 100 mg of HETM and 80 mg of $FeCl_3{\cdot}4H_2O$ were added. In continuation, after 20 min of stirring 80 mg of KNO_3 was introduced in the reaction solution and the mixture was heated up at 80 °C for 4 h. The reaction was left to cool down at room temperature and the resulted magnetically functionalized hollow NCs were purified by water via centrifugation [12,49]. After the incorporation of magnetic nanoparticles the structure of the microspheres has no considerable changes, except the fact that more raspberry-like structures are observed. Full characterization of the incorporated mNPs is included in the Supplementary file.

2.5.4. Synthesis of yolk-shell PMMA@P(MMA-co-HPMA-co-DS-co-DVB) Fe_3O_4@APTES@FITC core-shell NCs

To start with, 10 mg of the iron functionalized NCs were dispersed in a mixture solution of water/ethanol (10:50). Following, 100 μl APTES was added dropwise, then a catalytic amount of NH_3 was also added and the mixture was left under stirring for 4 h, at room temperature. The silica coated magnetic NCs were then collected by centrifugation, washed with EtOH twice and centrifuged again. The isolated material was dried under vacuum and then 4 mg were redispersed in dry DMF with catalytic amount of triethylamine (Et_3N). In another vial, 2 mg of fluorescein isothiocianate (FITC) and 50 μl of DIC were mixed in dry DMF and left under stirring at 0 °C for 30min. Afterwards, the mixture of activated fluorescein was added in the mixture NCs, under nitrogen, and the final mixture was left for overnight reaction. In order to purify the final product, the FITC functionalized NCs mixture was centrifuged and washed with DMF three times. The functionalization was further confirmed by confocal microscopy after FITC conjugation (Fig. S1B).

2.5.5. Synthesis of yolk-shell PMMA@P(MMA-co-HPMA-co-DS-co-DVB) Fe_3O_4@APTES@FA/FITC (tNCs)

In a mixture of DMF (1 ml) and Et_3N (10 μl), 4 mg of PMMA@P (MMA-*co*-HPMA-*co*-DS-*co*-DVB)Fe_3O_4@APTES@FITC NCs were dispersed. In another mixture of DMSO (0.5 ml) and DIC (50 μl) 3.4 mg of folic acid was dissolved under nitrogen and the solution was left for 30 min under stirring, in order for the reaction to be completed. The suspended NCs were then added dropwise in the mixture, which was left overnight under stirring. The reaction mixture was centrifuged, aiming at the isolation of the solid material. The unconjugated folic acid remained in the supernatant and its percentage was determined by UV–Vis via the standard curve method. From the difference between the final and initial concentration of folic acid in the supernatant, it was possible to calculate the amount that actually conjugated onto the NCs (0.39 μg/mg of the polymer).

2.6. Loading and release study

In order to investigate the tNCs loading capacity (LC%) and their encapsulation efficiency (EE%) we used the anthracycline drug DOX as a model drug. The procedure is as follows; equal amounts of tNCs (5 mg) and DOX (5 mg) were suspended in phosphate buffer saline (PBS, 5 ml) at pH = 7.4. The mixture was left under gentle stirring for three days in the dark, at room temperature. The mixture was then isolated and the supernatant was removed. In a second step of purification, the nanocontainers were resuspended in PBS (5 ml) and then the mixture was centrifuged again. The second supernatant was removed also. This purification method was repeated twice. The drug release was assumed to start as soon as the containers were suspended. The concentration of loaded NCs and released DOX from tNCs was quantified by using UV–vis spectroscopy, while the loading of DOX was further confirmed by confocal microscopy (Fig. S2A).

2.7. Characterization

2.7.1. Morphological and structural characterization

The following SEM and TEM images depict the resulting functionalized tNCs. The size of the tNCs is approximately 308 ± 16.21 nm and the sample is monodispersed. The NCs core surface is smooth, while after the shell growth the surface increases in size and becomes rougher. The observed outer layer cavity of the tNCs is due to shell collapse stemming from an internal cavity that was created during shell formation [11,12,16,46,49]. The cavity inside the spheres is verified through TEM images (Figs. 1 and 2). The black dots on the surface of the nanocontainers (Fig. 1D) are the embedded iron oxide nanoparticles with a mean size of 22.43 ± 3.93 nm.

According to DLS study the NCs behave in the desired way; when pH is increased the NCs' size augments significantly which indicates pH sensitivity of the structure. This phenomenon can be justified by the protonation/deprotonation equilibrium (pKa of Hydroxyl HPMA group is almost 6). In lower pH values, the hydroxylic acid groups are protonated (Fig. S3) whereas at higher pH values they are deprotonated causing the swelling of the NCs due to repulsive interactions.

According to these findings, the NCs can function as an ideal pH responsive drug delivery system, because the NCs' protonation in this environment can lead to the release of the encapsulated drug (Fig. S2B). As has already mentioned different interactions have been performed like hydrogen bonding and electrostatic interactions. Based on that at

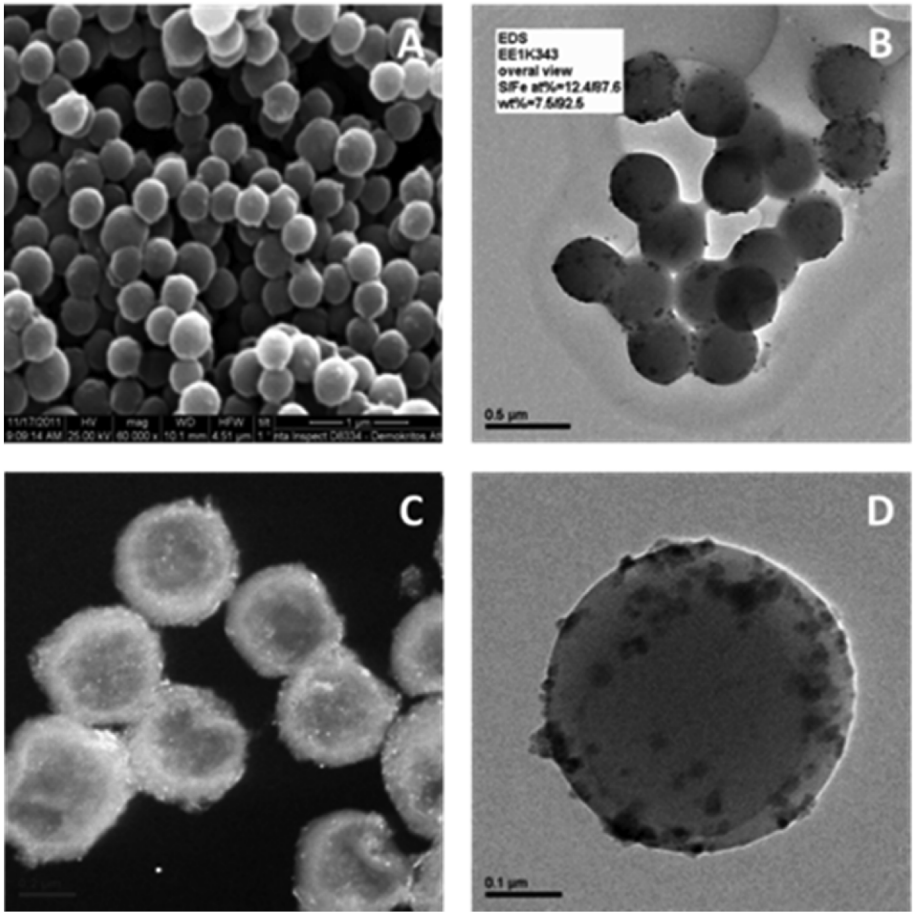

Fig. 1. Morphological characterization of functionalized NCs (tNCs), A) SEM image (size 300 ± 30 nm), B) TEM image of hollow tNCs, C) White field image of tNCs, D) focused TEM image of hollow tNCs.

slightly basic pH (pH = 7.4) the amine group of the drug is protonated and the hydroxyl group is deprotonated so maximum electrostatic interaction have been created. When the pH is acidic (pH 4.5) the drug and the NCs remain protonated and repulsed releasing the drug. The redox environment can function as a selective environment for cancer cells in which the concentration of GSH is 10 folds higher that in healthy cells. Based on that the treatment of NCs with GSH in neutral environment is to avoid the oxidation of GSH. Fig. 3 depicts the release of DOX under different pH, Temperature and Redox conditions. In order to investigate how the redox environment affects the drug release, the tNCs were treated at slightly basic pH with GSH. This study took place in basic environment to ensure the highest GSH affection. The structural characterization of the NCs has been carried out by the FT-IR spectroscopy. Fig. S1 depicts the spectra of core, core-shell, hollow and functionalized NCs. Two characteristic absorbance peaks were observed at 1530 cm^{-1} and 1687 cm^{-1} wave numbers, which correspond to the absorbance of the benzene loop of folate and the amide bond (–CO–NH-) formation respectively [34]. The symmetric and asymmetric C═S stretching vibrations at 730 and 1417 cm^{-1} confirmed the formation of thiourea group in the Fitc conjugation. Furthermore, a peak at 3435 cm^{-1} related to the NH_2 stretching was detected. The absorption at 580 cm^{-1} is characteristic of Fe–O bond vibration [34,50,51].

2.8. In vitro study

2.8.1. In vitro cytotoxicity

Human Caucasian breast adenocarcinoma cell line (MCF-7) and Human epithelial cervical cell line (HeLa) were cultivated in DMEM medium, containing 10% FBS, 2 mM L-glutamine, 100 μg/ml penicillin, and 100 μg/mL streptomycin. The incubation environment was at 37 °C supplemented with 5% CO_2 atmosphere. Both cell lines grew as monolayers.

The growth inhibition of MCF-7 and HeLa cells for all compounds was tested by using the MTT assay as described elsewhere [52]. Briefly, cancer cells were seeded in 96-well plates (1.5 x 10^4 cells in 100 μl of medium/well) in triplicate, allowed to grow overnight, and then treated with tested compounds for 24 h. After incubation, the medium was replaced with 100 μL of 1 mg/mL 3-(4,5-dimethylthiazol-2-yl)-2,5-diphenyl tetrazolium bromide (MTT) solution and the plate was incubated for another 4 h. The dark-blue formazan crystals which precipitate by viable cells were dissolved in 100 μL of DMSO. Results are expressed as percentage (%) of treated cells versus untreated cells, using data from three independent experiments that had each been repeated two times.

Cells were incubated in various concentrations of free DOX, DOX-loaded NCs and empty NCs as well as tNCs with and without drug (ranging from 0.1 to 100 μM for DOX and 0.1–39 μg/mL for NCs.

2.8.2. Confocal microscopy

Each cell line (5 *10^6 cells/well) was grown on 0.22 cm^2 coverslips which were then inserted into a six well plate containing DMEM and incubated for 24 h at 37 °C. Upon treatment of cells with Fitc or Fitc/Folic tNCs [35] the incubation lasted 30 min at 37 °C. For co-localization studies, 100 nm LysoTracker™Red was added for the last 10 min of treatment. Following, the cells were washed three times with PBS and prepared for confocal imaging. Confocal images were edited with the Confocal Assistant software.

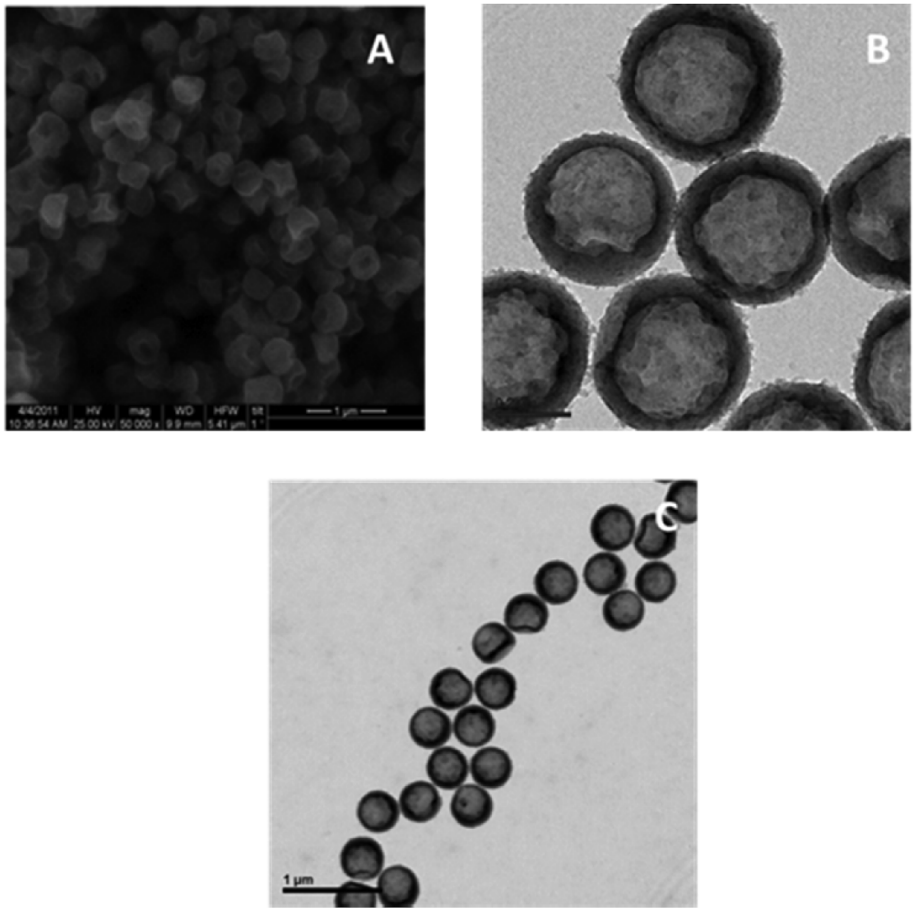

Fig. 2. Morphological characterization of hollow tNCs, A) SEM image of cavity formation into tNCs (size 300 ± 30 nm), B) TEM image of tNCs, C) cavity formation of tNCs (Yolk type).

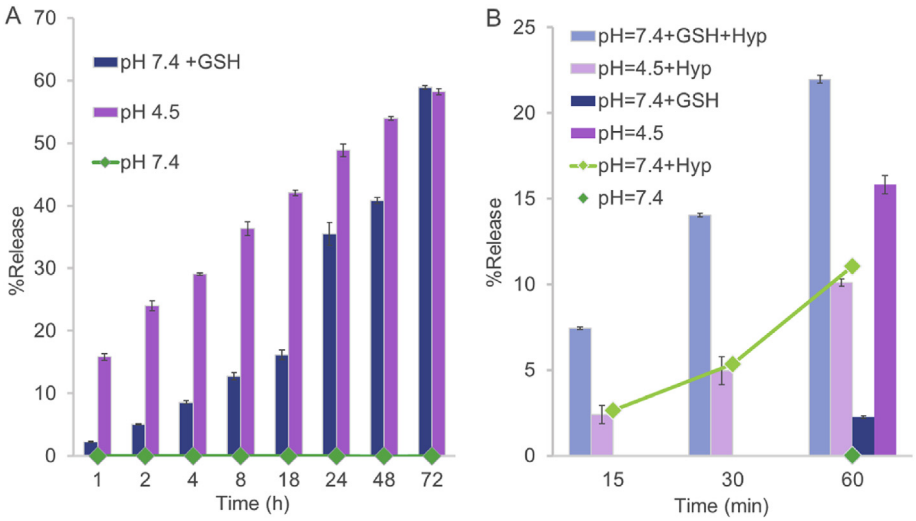

Fig. 3. tNCs@DOX release study under A) pH + RedOx stimuli, B) pH + RedOx stimuli under the application of hyperthermia.

2.8.3. Fluorescent microscopy

Each cell line (5 *10^6 cells/well) was grown on 0.22 cm^2 coverslips which were then inserted into a six well plate containing DMEM for 24 h at 37 °C. The incubation of cells exposed in DOX and Fitc/Folic-Dox loaded nanocontainers (10 μM to DOX concentration) was for 4 h at 37 °C. The cells were then washed three times with PBS and kept in the final PBS solution for fluorescence imaging. Fluorescent images were merged after taking the images in two filters (Fitc and red) and then co-localized.

2.9. In vivo investigation of targeting ability and therapeutic efficacy of tNCs and free NCs

2.9.1. In vivo studies of targeting ability

The targeting ability study was conducted at the Institute of Nanoscience and nanotechnology at the National Center of Scientific

Research "Demokritos". Eighteen female Nonobese Diabetic/Severe Combined Immunodeficient NOD/SCID mice (average weight 20 ± 2 g) were randomly allocated into three groups. Group A (n = 6) was the control group (animals without tumor) receiving radiolabeled NCs, Group B (n = 6) tumor bearing animals receiving radiolabeled NCs (10 μg HPMA displaying a radioactivity of 3.7 MBq) and Group C (n = 6) tumor bearing animals receiving tNCs (10 μg HPMA and 3,9 μg FA/100 μl displaying a radioactivity of 3.7 MBq). All animals were housed in cages under positive pressure in polysulfone type IIL individual ventilated cages (Sealsafe, Tecniplast, Buguggiate, Italy). Room temperature and relative humidity were 23 ± 2 °C and 55 ± 10% respectively. Mice had *ad libitum* access to water and food. Group B and C were xenografted at three weeks of age with HeLa cells subcutaneously at the right side of the thorax. Tumors were inoculated after injection of $6*10^6$ HeLa cells in NOD/SCID mice, which were previously grown in DMEM. After one month, when the first macroscopical presence of tumor was evident, Group A and B subjected in intravenous administration from lateral coccygeal vein of 0.1 ml of radiolabeled NCs (10 μg in 0.1 ml) while Group C of 0.1 ml of tNCs (10 μg in 0.1 ml) also radiolabeled. For the i.v. injections the animals were restrained in an acrylic restrainer and their tail was immersed in lukewarm water in order to achieve vasodilation.

2.9.1.1. Conjugation of ^{99m}Tc (via direct labelling) with tNCs/NCs. Radiolabeling was performed with ^{99m}Tc *via* a direct labelling method using stannous chloride $SnCl_2$ as the reducing agent as previously described by Psimadas et al. [53] Briefly, 100 μl of a fresh $Na^{99m}TcO_4$ generator eluate (1–2 mCi) was reduced by adding a volume of 40 μl $SnCl_2$ solution (1 mg/ml in 0.5 N HCl). The pH of the mixture was immediately adjusted to 7 using sodium hydrogen carbonate solution $NaHCO_3$ (0.5 M). Thereinafter, an aliquot of 20 μl of the NCs' suspension (1 mg/ml) was added and the mixture was gently stirred and allowed to react at room temperature for 30 min. Radiochemical analysis of the labeled tNCs was determined by ITLC using silicic acid coated fiber sheets [54].

2.9.1.2. Biodistribution analysis by γ-imaging. All animals were investigated by γ-imaging. Evaluation of the novel SPECT radiolabeled NCs was performed by dynamic imaging studies using a high resolution, small animal dedicated, gamma-camera. Half of the animals from each group were subjected to the respective i.v administration and 1 h afterwards the NCs or tNCs biodistribution was evaluated (0.1 ml of each, equal to 10 μg radiolabelled materials). Similarly, the rest of the animals were investigated at 24 h post administration. The animals were anesthetized by a solution of xylazine/ketamine in saline 0.9%: 0.25 ml of xylazine (20 mg/ml) and 0.5 ml of ketamine (100 mg/ml) were mixed with 4.25 ml of saline. A volume of 0.1 ml/10 gr body weight was administered i.p. prior to scanning. Then the mice were positioned to the animal bed at a distance of less than 1 cm from the camera head, to allow imaging with maximum spatial resolution. All the 2 min successive frames were summed and the regions of interest were drawn (ROIS). Then those ROIs were applied to the 2 min frames, to provide semi-quantitative time activity curves [38,55]. At the end of the procedure all animals were euthanized under anesthesia and exsanguination and samples of blood, muscle and urine were collected additionally, their organs were harvested, weighed and counted, in a γ-counter system. In comparison to a standard of the injected solution, results were expressed as a percentage of the injected dose (%ID) per organ and per gram of each organ or tissue. For total blood radioactivity calculations, blood was assumed to be 7% of the total body weight [38,55].

2.9.2. In vivo evaluation of therapeutic efficacy of tNCs

The *in vivo* investigation of the therapeutic efficacy took place at the Centre for Experimental Surgery of the Biomedical Research Foundation of the Academy of Athens. Thirty female NOD/SCID mice were inoculated with HeLa cells as previously described. The animals were housed 6 in cages under positive pressure in polysulfone type IIL individual ventilated cages (Sealsafe, Tecniplast, Buguggiate, Italy). Room temperature and relative humidity were 24 ± 2 °C and 55 ± 10% respectively. All animals in the facility are screened regularly according to the Federation of European Laboratory Animal Science Associations' recommendations and were found free of the respective pathogens. Mice had *ad libitum* access to water and food.

All groups received intravenous administration at the lateral coccygeal vein of 0.1 ml once a week for the study period. For *i.v.* administration the animals were restrained in an acrylic restrainer and their tail was immersed in lukewarm water in order to achieve vasodilation. The animals were randomly allocated into 5 groups; Control group receiving saline 0.9% and the other groups were injected with 2 mg/ml on the DOX (The injected amount about NCs and tNCs was calculated to be total 2 mg/ml of DOX). Group 1 receiving DOX, Group 2 receiving NCs@DOX, Group 3 receiving tNCs@DOX and Group 4 receiving tNCs@DOX under hyperthermia (f = 163 Hz, I = 415,5 A, t = 30 min, coil diameter 4.1 cm, 6 spiral). Humane endpoints were predetermined (tumor volume over 1,2 cm for severe compromise of the welfare of the animals and body weight loss over 20%). The tumor volume and mice weight were monitored once a week with an automatic caliper and scale. The tumor volume, body weight and the survival rate were calculated in different time intervals. Mice of Group 4 were treated by alternate magnetic field for 30 min under anesthesia. A solution of xylazine/ketamine in saline 0.9% was prepared: 0.25 ml of xylazine (20 mg/ml) and 0.5 ml of ketamine (100 mg/ml) were mixed with 4.25 ml of saline. A volume of 0.1 ml/10 gr body weight was administered i.p.

Ethical statement. All protocols were approved by the General Directorate of Veterinary Services Athens, Greece according to Greek legislation (Presidential Degree 160/1991) in compliance with the European Economic Community Directive 609/1986, and Law 2015/1992 for the protection of vertebrate animals used for experimental or other scientific purposes, 123/1986.

3. Results & discussion

The different steps of the synthesis of Fitc and/or folic acid modified NCs are summarized below. In the first step the core was synthesized and in a second step the shell with the desired properties was fabricated. In the third step amino-silane was used to introduce amino groups on the NCs' surface. After that, fitc and/or folic acid were conjugated on the NCs through carbodiimide chemistry (Scheme 1). In each step the resulted product was isolated, purified and fully characterized. The amount of conjugated folic acid was calculated by the standard curve method. The fitc modified NCs were used only for imaging application with the employment of confocal and fluorescence microscopy on HeLa cells.

3.1. Morphological, structural and hydrodynamic diameter characterization

The tNCs' morphology at each step of modification is presented in Fig. 1. As it is observed, the seed size is 200 nm and after the shell fabrication their diameter increases at 308 nm. In the TEM images the NCs diameter is depicted in solid state after the mNPs' doping. The mNPs' size was calculated by the Scherrer equation via XRD and the results were in good agreement with those delivered by TEM (Detailed information is available in the Supplementary file). However, the size values stemming from DLS measurements, deviate from the aforementioned TEM and XRD size values, which was expected considering that DLS measures the hydrodynamic diameter (Dh) of our samples. The hydrodynamic diameter ranges from 610 to 630 nm until temperature reaches approximately 38 °C. This decrease can be attributed to the thermo-sensitive segment of HPMA which, according to literature, has a

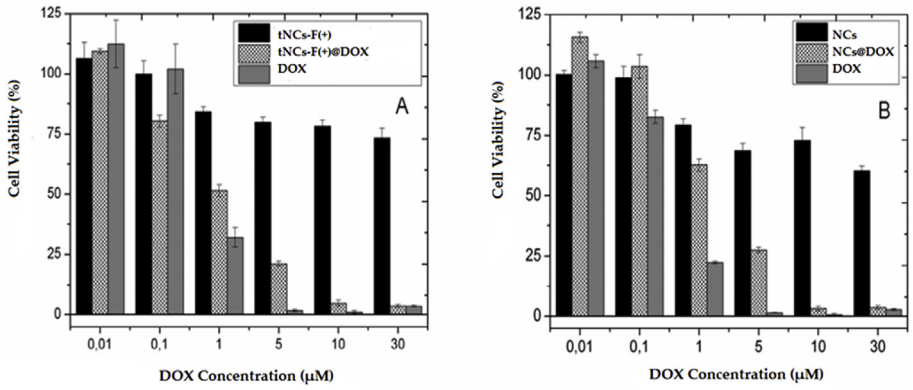

Fig. 4. Cytotoxicity profile, of empty NCs, tNCs, DOX-loaded targeted and not targeted NCs and free DOX, on HeLa cells (n = 3, the results expressed as % cell viability ± SD).

lower critical solution temperature at 38 °C [56]. Above this temperature, the thermo-sensitive segment becomes more hydrophobic and, in its effort, to avoid the aqueous environment causes a reduction in the microsphere's size. The zeta potential of the pH trend study ranges between −29 and −27 mV. According to this measurement the size increases when the pH decreases and this behavior differs when the pH increases. This behavior can be attributed to the protonation of hydroxylic groups at acidic pH values resulting in the swelling of tNCs, due to hydrogen bonds formation. The structural characterization of the tNCs was determined by FT-IR spectroscopy (Fig. S1). The peak at 555 nm cm^{-1} which was observed in the spectra of tNCs@mNPS, is characteristic of the Fe–O vibration and indicates that the iron deposition was successful. The peak noted at 1535 cm^{-1} in spectra b and c, can be assigned to the C–N stretching vibration from HPMA. The small peak at 710 cm^{-1} observed in spectra b and c, corresponds to the = C–H out of plane vibration of DVB [16,49] The peak at 1650 cm^{-1} is characteristic of the amide bond formation. The crystal structure of magnetite nanoparticles that were formed onto the tNCs' surface was identified by X-ray diffraction (XRD). Thermogravimetric analysis of tNCs revealed that 6.9% of the material consists of iron oxide nanoparticles and the rest is attributed to the organic material (Fig. S6).

According to the XRD study the phase of the nanoparticles is indicative for magnetite (Fe_3O_4) (Fig. S5), with a Ms value ~70emu/$g_{iron\ oxide}$. The values of Hc and Ms and the small size of the nanoparticles denote a superparamagnetic behavior. (Fig. S7) [16,49].

Magnetic hyperthermia experiments *ex vitro* in 1 ml solutions of 3 three different concentrations revealed that at 100 mg of tNCs/ml - corresponding to ~7 mg iron oxide nanoparticles-the desired heat dissipation is achieved reaching a temperature of ~43 °C.

3.2. Drug loading and release of tNCs

As previously described, tNCs were loaded with the anticancer drug doxorubicin in PBS solution (pH = 7.4 at 25 °C). Unbound DOX was removed by centrifugation and the concentration was calculated through standard curve method by UV–vis spectroscopy [3,11–13,16], thus the loaded drug amount per mg of the corresponding polymer was indirectly calculated; m = 479.9 ± 2.2 μg/mg (LC% = 92.3, and EE % = 92.3). The drug loaded tNCs were then lyophilized and stored in the dark at room temperature. The encapsulation mechanism is based on the electrostatic interactions between the protonated amino group of the drug (pKa = 8.4) and the deprotonated hydroxylic groups of tNCs, because of the HPMA participation in the shell composition. The release study took place in different conditions of pH, redox and hyperthermia by application of an external alternating magnetic field. As it is observed in Fig. 3A the drug was released at acidic pH in a prominent way indicating a sustained release profile (60% in 72 h), in contrast to neutral pH in which the release is low (2% in 72 h). Furthermore, different combinations of stimulus, such as pH, hyperthermia (heating) and glutathione were applied. In the case of the combined magnetic hyperthermia the induced temperature was at 42 °C, at pH 7,4 and in the presence of glutathione a substantial increase of the release rate was observed. The release at pH 4.5 with hyperthermia after 1 h treatment is about 12% and without hyperthermia at 16% indicating that hyperthermia does not affect the release at pH 4.5.(Fig. 3) Taking into account that these factors are present in a tumor, the tNCs exhibit a desirable behavior for the implementation of specific targeting therapy.

3.3. Cytotoxicity studies

The cytotoxicity of the NCs and tNCs both DOX-loaded and unloaded ones, was examined by the MTT assay [57]. In particular, the cytotoxicity of free DOX (0.01, 0.1, 1, 5, 10 and 30 μM) and DOX-loaded tNCs at the same drug concentrations were comparatively studied on the cell lines of MCF-7 human breast carcinoma and HeLa human cervix carcinoma. HeLa cells are known to recognize FA via the FA receptor (FR) attached to their surface. Once a ligand binds to the FR, the respective ligand–receptor complex is endocytosed and the receptor then recycles back to the cells' surface [26,27,34–37]. Moreover, the cytotoxicity of the non-drug loaded NCs, both FA targeted and non-targeted, was examined, in order to determine their potent and selective contribution to the cytotoxic effect. Therefore, the NCs concentrations employed in the cytotoxicity studies were based on the polymeric amount that contains the aforementioned DOX concentrations (0.012, 0.1, 1.0, 5.2, 10.4 and 31.3 μg/mL). The incubation time of the cells in the presence of NCs, with or without FA, in different concentrations was 72 h (Figs. 4 and 5). Our results show that even at high concentrations the empty NCs exert marginal toxicity on HeLa cells, whereas relevant toxicity is exerted when the same concentrations were tested on MCF-7 cells. It was observed that the IC_{50} for DOX is 0.2 and 0.7 μM for MCF-7 and HeLa cells, respectively. Once DOX is encapsulated in the NCs, its exerted cytotoxicity as a free drug is retained, with the observed IC_{50} value being significantly higher. This is observed in both tested cell lines, the FR positive (HeLa) and the FR negative (MCF-7) ones [21,23,27,34,36,37,44] This increase was also observed after testing the non-targeted NCs. Based on these findings, we can discern the targeting ability of our construct from the calculated relevant IC_{50} increase (Tables 1 and 2).

3.4. Folic acid targeting ability

3.4.1. Cell uptake of folate targeted and non-targeted NCs

To determine the targeting ability of folate functionalized tNCs on specific FR we used the human cervical carcinoma cell line HeLa, which overexpress the FR, indicated as a positive FR control and the human

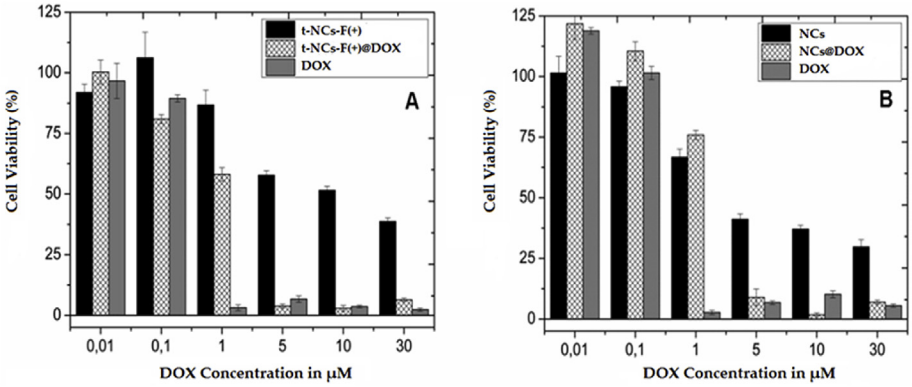

Fig. 5. Cytotoxicity profile of empty NCs, tNCs, DOX-loaded NCs targeted and not targeted and free DOX, on MCF-7 cells (n = 3, the results expressed as % cell viability ± SD).

Table 1
IC_{50} values of the loaded tNCs on HeLa cells.

Sample	IC_{50} (μM)
DOX	0.7 ± 0.05
tNCs/DOX	1.8 ± 0.12
NCs/DOX	2.5 ± 0.2

Table 2
IC_{50} values of the loaded tNCs on MCF-7 cells.

Samples	IC_{50} (μM)
DOX	0.2 ± 0.0012
tNCs/DOX	1.2 ± 0.021
NCs/DOX	1.8 ± 0.08

breast cancer cell line MCF-7 as a negative FR control [21,23,27,34,36,37,44]. From the previously described cytotoxicity studies, it is concluded that the folate functionalized tNCs present higher cytotoxicity on HeLa cells than on MCF-7 cells, in the same concentrations. These results were further supported by the confocal and fluorescence microscopy studies. The HeLa cancer cells were treated with folate/Fitc- and Fitc-functionalized NCs while monitoring their uptake for 30 min, as an ideal incubation time for targeting determination. After that, LysoTracker™Red was added the last 10 min of incubation. Following, the sample was washed three times with PBS and kept in DMEM media without FBS. Figs. 7 and 8, present the confocal imaging of live HeLa cells after uptake experiments of Fitc/Folic- and Fitc-functionalized NCs. As it is depicted the Folic/Fitc-functionalized NCs were attached on the surface of cancer cells, in contrast to the Fitc-functionalized NCs which were shown to be randomly distributed outside the cells. This observation confirms that the folate tNCs were attached on the cancer cell surface via the folic receptors and internalized creating lysosomes (Figs. 7 and 8) (red colored spots inside the cells) [58].

The lysosomes created indicate that the Folic/Fitc-functionalized tNCs internalized much more than the Fitc-functionalized ones. In Fig. 8B it is observed that the lysosome's formation is increased with the presence of the Folic/Fitc-functionalized tNCs. According to literature [26,27,35–37,39,44,50,59,60] it has already been established that folic acid is an ideal targeting moiety at certain concentrations for other nanoformulations. The optimum amount is at about 0.1–0.2 mmol folate/mg of the polymer, above which the uptake of the targeted polymer decreased. Based on these data, the amount of folate in our functionalized tNCs is about 0.34 mg Folate/mg of the polymer, which is an ideal amount for the desired targeting [29,35,58]. The above mentioned results were confirmed by fluorescent microscopy, which allows the observation of the functionalized tNCs' targeting ability.

Investigating the possible changes of the internalization mechanism of DOX loaded tNCs we treated HeLa cells with the DOX and DOX -loaded tNCs for 4 h. As it is depicted in Fig. 9A, free DOX can penetrate the cell membrane and then was localized in the nucleus, where it induces inhibition of the DNA replication by intercalation. Fig. 9B confirms that the targeting process does not affect the internalization pathway (Fig. 6). The green colored tNCs are located on the cell membrane in contrast with the drug which goes to the nucleus, which constitutes the red colored area. According to the presented results the encapsulated DOX localization after 4 h of treatment was observed inside the nucleus as the free DOX, which implies that the DOX distribution inside the cell is not affected by the polymeric matrix of the NCs. (Fig. 10) Taking into consideration all the *in vitro* experiments, it was concluded that in maximum 1 h we can succeed to target the folate overexpressing cells, like HeLa which are used as the FR positive, while the drug release can be counted as sustainable improving the circulation time in the organisms [35].

3.5. In-vivo investigation of tNCs

3.5.1. Radiolabeling-radiochemical analysis

Radiolabeling of the NCs with ^{99m}Tc was performed by the direct labelling approach. A two-strip ITLC-SA method for the analysis of HPMA-FR positive/HPMA-FR negative showed that no amount of either pertechnetate $^{99m}TcO_4$ or of colloidal ^{99m}Tc was present. The radiochemical yield for both NCs was higher than 95%, providing a single radioactive species, as detected by Paper Chromatography (ITLC-SA)) (see Fig. 10).

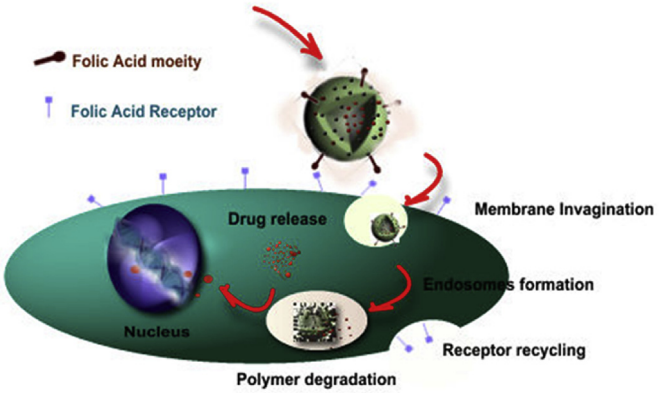

Fig. 6. Schematic representation of folic acid mediated endocytosis mechanism of tNCs.

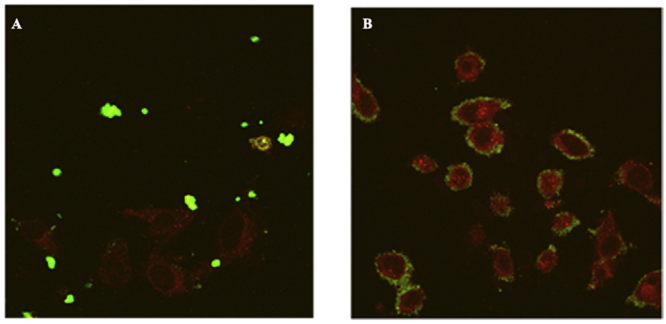

Fig. 7. Confocal images of live HeLa cells incubated for 30 min with fitc (A) and folic/fitc (B) functionalized NCs at 37 °C, 5% CO_2 in the presence of LysoTracker™Red (cells treated by Lyso Tracker for 10 min). In both experiments the cell were treated with 10 μg/ml of functionalized tNCs.

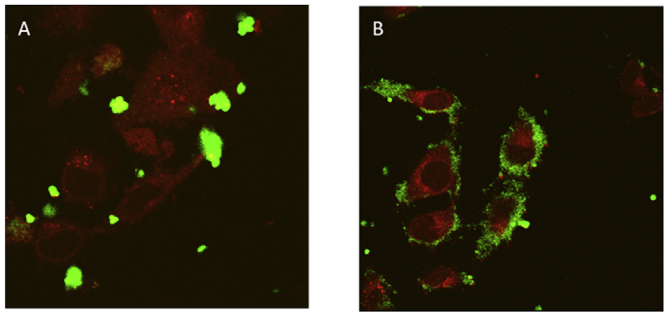

Fig. 8. Focused confocal images of A) Fitc-NCs, B) Folic/Fitc-functionalized NCs.

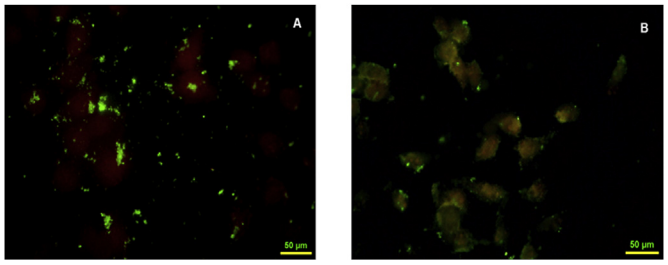

Fig. 9. Cellular trafficking of FITC-(A) and FA/FITC-labeled (B) NCs in HeLa cells. The cells were incubated for 1 h with the FITC-labeled NCs in the presence of LysoTracker™Red (10 min) at 37 °C, followed by live cell imaging.

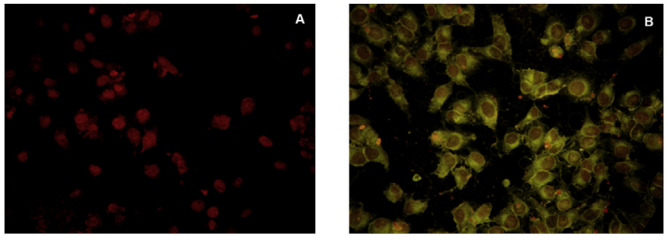

Fig. 10. Cellular trafficking of DOX (A) and FA/FITC-DOX loaded (B) tNCs in HeLa cells. The cells were incubated for 4 h with the FA-FITC-labeled NCs at 37 °C, followed by live cell imaging. In both experiments the cell were treated with 10 μg/ml of functionalized tNCs.

3.5.2. *Biodistribution analysis and dynamic γ-camera imaging in mice*

The biodistribution studies (Fig. 11 and Fig. 12 and the scintigraphy Fig. 13), performed by radiolabeling the tNCs and NCs with 99mTc, revealed enhanced uptake at the tumor site via FR-mediated endocytosis for tNCs (3.5 ± 0.24% ID/g) versus NCs (0.5 ± 0.17% ID/g). Furthermore, the tumor-to-blood ratios (0.71) and tumor–to-muscle ratios (8.97) were higher for tNCs than for NCs (0.13 and 1.51 respectively), at 1 h p.i. However, the uptake of tNCs was much more clearly delineated at the early time point of 10 min p.i. (according to the imaging studies) than at 1 h p.i. For both NCs the highest %ID was observed at the organs of reticuloendothelial system (RES i.e. liver, spleen, lungs) for all groups possibly due to aggregate formation. Higher kidney and lung uptake of tNCs was observed probably because of folate receptor expression in these organs (Figs. 11-14).

3.5.3. *In vivo tumor efficacy of NCs and tNCs in HeLa tumour bearing mice*

To evaluate the tumor efficacy of NCs and tNCs loaded with the anticancer drug DOX in combination with hyperthermia treatment, SCID mice were inoculated with HeLa cells [1,30,54,61–64]. The animals were randomly divided in five groups and injected with the above mentioned formulations via the lateral coccygeal vein once a week. The injected dose was fixed at 5 mg/ml and the tumor volume was measured by using the equation below

$$V\ (mm^3) = a*b^2$$

were a and b are the major and minor axes of the tumor.

Fig. 14 demonstrates the results of tumor efficacy and the NCs ability to administrate higher amount of DOX to the site of interest than the drug itself by simultaneously avoiding the toxicity normally induced by free DOX. From the results of the targeted therapy studies, it can be deduced that the tumor volume decreases during the thirtieth day of treatment.

According to Fig. 14 it is obvious that the tumor volume of the animals which were treated with PBS, referred to as Group 1 (Blue line), increases as a function of time and treatment. Group 2 (treated with free DOX) survived for 18 days, while the tumor volume increased. Group 3 and 4 the DOX loaded NCs and tNCs presented a different mode of action. In detail Group 3 (DOX loaded non-targeted NCs) showed similar behavior with free DOX. It is worth mentioning that the tumor volume remained stable for 30 days and then increased while the animals survived for 37 days. In contrast, the DOX loaded tNCs (Group 4) exhibited improved anti-tumor efficacy by decreasing the tumor volume within 30 days. After this period the tumor increased in a small degree. Group 5, mice treated with tNCs and Magnetic Hyperthermia (Fig. 15), also showed slightly more tumor shrinkage than Groups 4 and 3. In all cases the animals' weight remained stable, whereas following free DOX treatment the animals lost weight during therapy, suggesting the increased free DOX toxicity. These results support the hypothesis behind the NCs concept of sustained release mechanism, which can play a crucial role both in therapeutic efficacy and in reduced toxicity.

According to Fig. 16 only in Group 2 body weight decreased indicating the toxicity of the free drug. Group 5 (the DOX loaded tNCs under hyperthermia) had increased delay in the tumor growth in contrast to Group 2.

Compared to Group 1, in groups 4 and 5, tumor growth was effectively inhibited during therapy. The groups treated with tNCs exhibited a better response to those treated with free DOX and non-targeted NCs. Fig. 16 shows body weight variations in all 5 groups during the tumor efficacy protocol. In detail, Group 2 showed a significant decrease in body weight compared with the control group as well as the other groups. These results are in good agreement with the literature in which is referred that DOX cause higher toxicity on the administered corresponding Group [65]. On the 3rd week Group 2 had a dramatic decline of their body weight compared to baseline. Animals treated with DOX loaded tNCs continued to gain weight.

According to Kaplan – Meier survival curves (Fig. 17), Group 2 died possibly due to severe toxicity, whereas the other groups, survived during the period of observation.

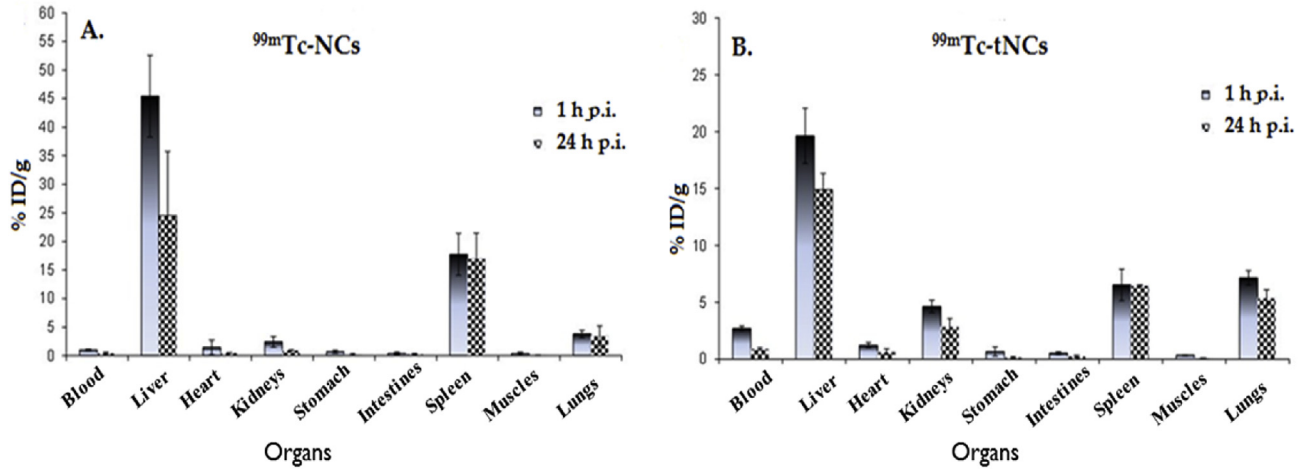

Fig. 11. *In vivo* uptake at 1 h and 24 h post injection (p.i.) for the radiolabelled NC (A) and tNC (B) intravenously injected in Group A. Biodistribution values represent the mean ± standard deviation of %ID/g.

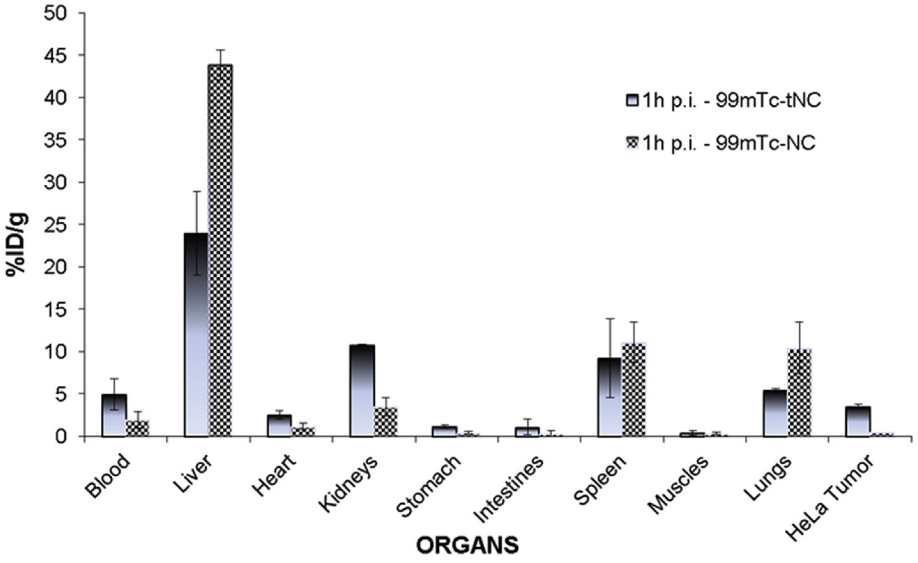

Fig. 12. *In vivo* uptake at 1 h post injection (p.i.) for the radiolabelled of NCs and tNCS intravenously injected in groups B and C. Biodistribution values represent the mean ± standard deviation of %ID/g.

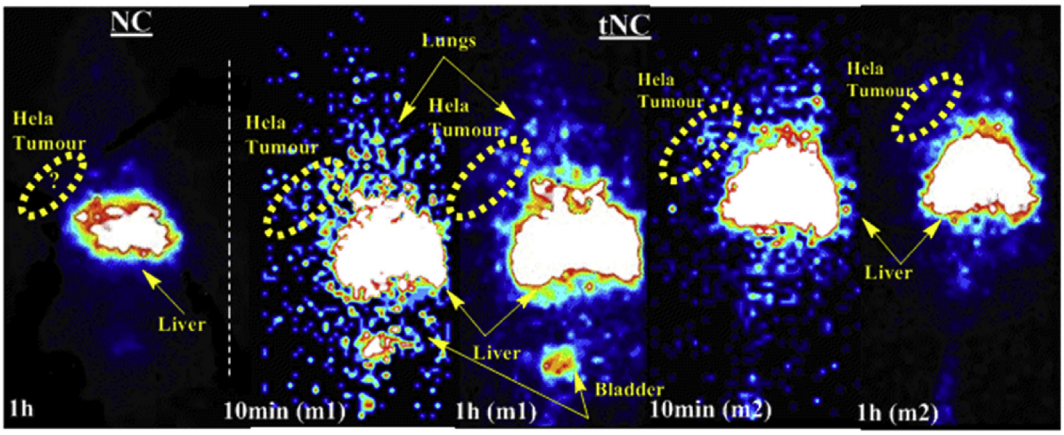

Fig. 13. Scintigraphic image at 1 h post-injection of one animal from Group B Scintigraphic images at 10 min p.i. and at 1 h p.i. of two animals from Group C.

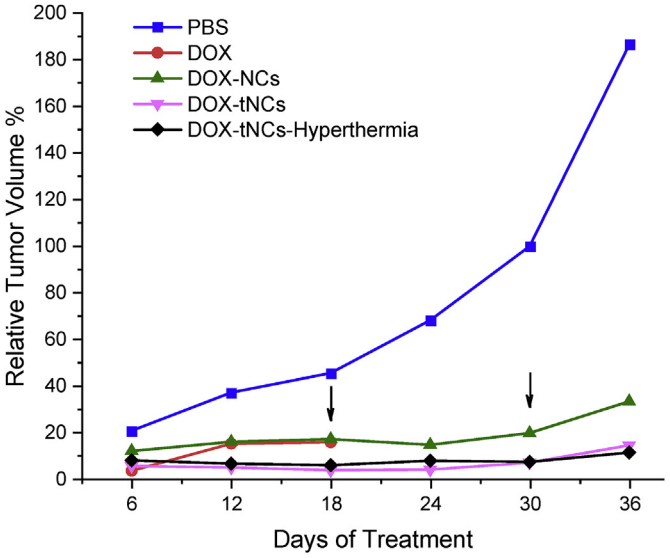

Fig. 14. Antitumor activity of free drug, loaded NCs and tNCs under hyperthermia in comparison with PBS treatment.

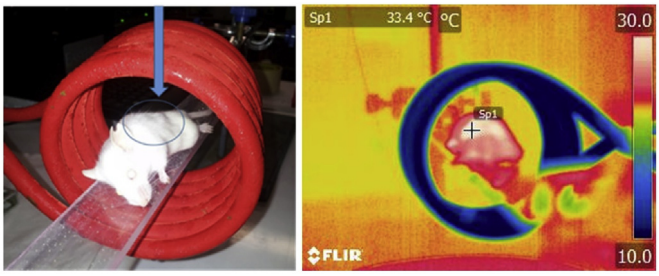

Fig. 15. Hyperthermia application during chemotherapy.

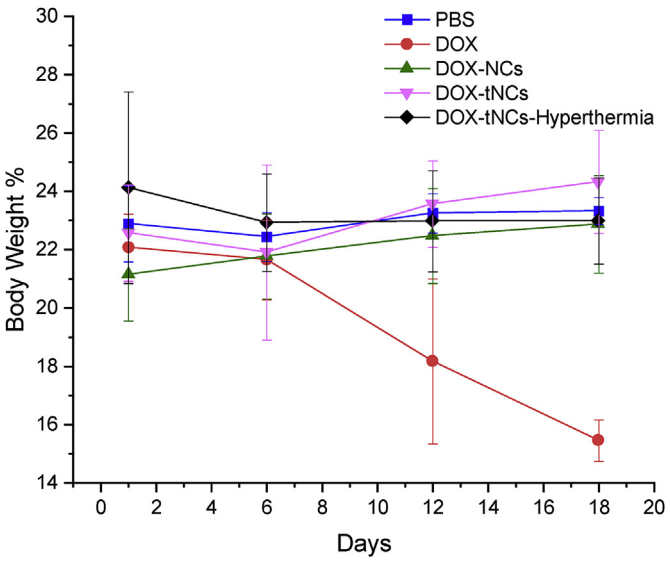

Fig. 16. Relative weight changes of mice after i.v. injections with: saline (control group), DOX, DOX loaded NCs, DOX loaded tNCs, and DOX loaded tNCs in the presence of hyperthermia (n = 6 per group, results expressed as weight ± SD).

4. Conclusions

In this study, functionalized multi stimuli NCs that can be used as FR positive targeted drug delivery system with *in vitro* and *in vivo* applications are presented. These tNCs in combination with hyperthermia exhibit superior antitumor activity in HeLa tumor bearing mice, than free DOX, while maintaining decreased toxicity by exploiting specific tumor characteristics.

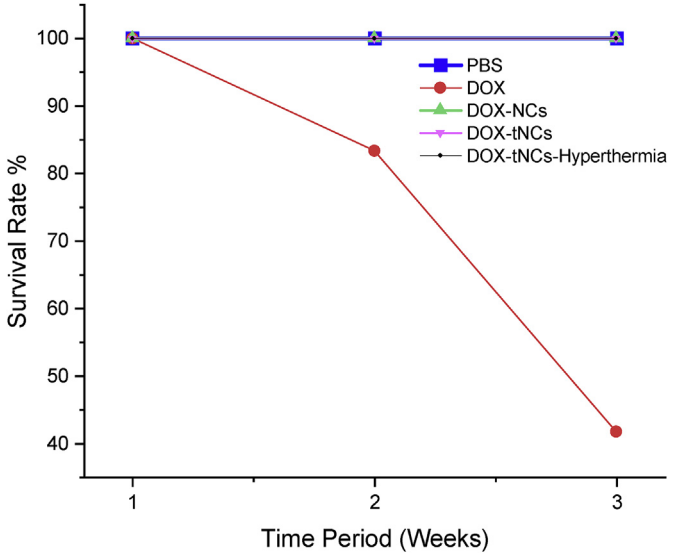

Fig. 17. Survival rate by Kaplan-Meier equation analysis.

This system can be characterized as an ideal delivery carrier for an anticancer drug in order to transport the drugs specifically to cancer cells and release the drug molecules inside the cells resulting in the enhancement of drugs' the anticancer activity. Further investigation is needed in order to conclude if these highly desirable effects are applicable to humans. According to our results the tNCs targeted HeLa cells' surface at the first 30 min. Human tumor xenografted SCID mice were injected with the tNCs and their tumor uptake was estimated by γ-imaging at about 3.5%. Tumor efficacy experiments have also been done aiming at determining the therapeutic ability of the fabricated system. These results concerning the tNCs exhibiting negligible toxicity, indicates the excellent targeting and cellular internalization ability which can lead to cell apoptosis in tumors.

Declaration of competing interest

The authors declare that they have no known competing financial interests or personal relationships that could have appeared to influence the work reported in this paper.

Acknowledgments

This work was supported by European Research Council (ERC) for financial support of this work under the "POC" project called "A Novel Micro-container drug carrier for targeted treatment of cancer" with the acronym NANOTHERAPY and the reference number 620238.

Appendix A. Supplementary data

Supplementary data to this article can be found online at https://doi.org/10.1016/j.jddst.2019.101481.

References

[1] L.W. Xiang, Bioconjug. Chem. 21 (2010) 208–213, https://doi.org/10.1021/bc9005283.
[2] T.M. Allen, E.H. Moase, Adv. Drug Deliv. Rev. 21 (1996) 117–133.
[3] P. Bilalis, E.K. Efthimiadou, A. Chatzipavlidis, N. Boukos, G. Kordas, Polym. Int. 61 (2012) 888–894.
[4] I. Brigger, C. Dubernet, P. Couvreur, Adv. Drug Deliv. Rev. 54 (2002) 631–651.

[5] J.-F. Chen, H.-M. Ding, J.-X. Wang, L. Shao, Biomaterials 25 (2004) 723–727.
[6] J. Cheng, Y.-J. Gu, S.H. Cheng, W.-T. Wong, J. Biomed. Nanotechnol. 9 (2013) 1362–1369.
[7] J.E. Chung, M. Yokoyama, T. Okano, J. Control. Release 65 (2000) 93–103.
[8] X. Yang, L. Chen, B. Han, X. Yang, H. Duan, Polymer 51 (2010) 2533–2539.
[9] D.K. Yi, S.S. Lee, G.C. Papaefthymiou, J.Y. Ying, Chem. Mater. 18 (2006) 614–619.
[10] J. Zhang, R.D. Misra, Acta Biomater. 3 (2007) 838–850.
[11] E.K. Efthimiadou, C. Tapeinos, P. Bilalis, G. Kordas, J. Nanoparticle Res. 13 (2011) 6725–6736.
[12] E.K. Efthimiadou, C. Tapeinos, A. Chatzipavlidis, N. Boukos, E. Fragogeorgi, L. Palamaris, G. Loudos, G. Kordas, Int. J. Pharm. 461 (2014) 54–63.
[13] E.K. Efthimiadou, L.A. Tziveleka, P. Bilalis, G. Kordas, Int. J. Pharm. 428 (2012) 134–142.
[14] K. Cho, X. Wang, S. Nie, Z.G. Chen, D.M. Shin, Clin. Cancer Res. Off. J. Am. Assoc. Canc. Res. 14 (2008) 1310–1316.
[15] M. Allmeroth, D. Moderegger, D. Gundel, H.G. Buchholz, N. Mohr, K. Koynov, F. Rosch, O. Thews, R. Zentel, J. Control. Release: Off. J. Contr. Release Soc. 172 (2013) 77–85.
[16] E.K. Efthimiadou, C. Tapeinos, L.A. Tziveleka, N. Boukos, G. Kordas, Mater. Sci. Eng. C, Mater. Biol. Appl. 37 (2014) 271–277.
[17] S.H. Yuk, S.H. Cho, S.H. Lee, Macromolecules 30 (1997) 6856–6859.
[18] C.M. Peterson, J.G. Shiah, Y. Sun, P. Kopeckova, T. Minko, R.C. Straight, J. Kopecek, Adv. Exp. Med. Biol. 519 (2003) 101–123.
[19] J. Kopecek, Eur. J. Pharm. Biopharm. 50 (2000) 61–81.
[20] J. Kopecek, P. Kopeckova, Adv. Drug Deliv. Rev. 62 (2010) 122–149.
[21] M.P. Borgman, A. Ray, R.B. Kolhatkar, E.A. Sausville, A.M. Burger, H. Ghandehari, Pharm. Res. 26 (2009) 1407–1418.
[22] J. Bushman, A. Vaughan, L. Sheihet, Z. Zhang, M. Costache, J. Kohn, J. Control. Release: Off. J. Contr. Release Soc. 171 (2013) 315–321.
[23] Z.Y. Chen, K. Liang, R.X. Qiu, J. Exp. Clin. Cancer Res.: CR (Clim. Res.) 29 (2010) 152.
[24] Y. Kotsuchibashi, Y. Zhang, M. Ahmed, M. Ebara, T. Aoyagi, R. Narain, J. Biomed. Mater. Res. A 101 (2013) 2090–2096.
[25] M.A. Phillips, M.L. Gran, N.A. Peppas, Nano Today 5 (2010) 143–159.
[26] F.-H.L. Shu-Jyuan Yang, Kun-Che Tsai, Ming-Feng Wei, Han-Min Tsai, Jau-Min Wong, M.-J. Shieh, Bioconjug. Chem. 21 (2010) 679–689.
[27] Z. Wang, B. Xu, L. Zhang, J. Zhang, T. Ma, J. Zhang, X. Fu, W. Tian, Nanoscale 5 (2013) 2065–2072.
[28] M. Ekkapongpisit, A. Giovia, C. Follo, G. Caputo, C. Isidoro, Int. J. Nanomed. 7 (2012) 4147–4158.
[29] H.S. Oberoi, N.V. Nukolova, F.C. Laquer, L.Y. Poluektova, J.G. Huang, Y. Alnouti, M. Yokohira, L.L. Arnold, A.V. Kabanov, S.M. Cohen, T.K. Bronich, Int. J. Nanomed. 7 (2012) 2557–2571.
[30] A. Remesh, Int. J. Basic Clin. Pharmacol. 1 (2012) 2.
[31] F.M. Safdie, T. Dorff, D. Quinn, L. Fontana, M. Wei, C. Lee, P. Cohen, V.D. Longo, Aging 1 (2009) 988–1007.
[32] H.I. El-Sayyad, Int. J. Biol. Sci. (2009) 466–473.
[33] Can. Vet. J. 50 (2009) 665–668.
[34] Hong Yang, Changchun Lou, Mingming Xu, Chunhui Wu, Hirokazu Miyoshi, Y. Liu, Int. J. Nanomed. 6 (2011).
[35] N.V. Nukolova, H.S. Oberoi, S.M. Cohen, A.V. Kabanov, T.K. Bronich, Biomaterials 32 (2011) 5417–5426.
[36] E. Roger, S. Kalscheuer, A. Kirtane, B.R. Guru, A.E. Grill, J. Whittum-Hudson, J. Panyam, Mol. Pharm. 9 (2012) 2103–2110.
[37] A. Rollett, T. Reiter, P. Nogueira, M. Cardinale, A. Loureiro, A. Gomes, A. Cavaco-Paulo, A. Moreira, A.M. Carmo, G.M. Guebitz, Int. J. Pharm. 427 (2012) 460–466.
[38] I. Tsiapa, E.K. Efthimiadou, E. Fragogeorgi, G. Loudos, A.D. Varvarigou, P. Bouziotis, G.C. Kordas, D. Mihailidis, G.C. Nikiforidis, S. Xanthopoulos, D. Psimadas, M. Paravatou-Petsotas, L. Palamaris, J.D. Hazle, G.C. Kagadis, J. Colloid Interface Sci. 433 (2014) 163–175.
[39] A.F. Metaxa, E.K. Efthimiadou, N. Boukos, E.A. Fragogeorgi, G. Loudos, G. Kordas, J. Colloid Interface Sci. 435 (2014) 171–181.
[40] C.G. Hadjipanayis, M.J. Bonder, S. Balakrishnan, X. Wang, H. Mao, G.C. Hadjipanayis, Small 4 (2008) 1925–1929.
[41] G. Bellizzi, O.M. Bucci, (2018) 129-191.
[42] J.F. Mano, Adv. Eng. Mater. 10 (2008) 515–527.
[43] B. Wang, X.D. Xu, Z.C. Wang, S.X. Cheng, X.Z. Zhang, R.X. Zhuo, Colloids Surfaces B Biointerfaces 64 (2008) 34–41.
[44] S. Mohapatra, S.K. Mallick, T.K. Maiti, S.K. Ghosh, P. Pramanik, Nanotechnology 18 (2007) 385102.
[45] M. Zhang, Y. Lan, D. Wang, R. Yan, S. Wang, L. Yang, W. Zhang, Macromolecules 44 (2011) 842–847.
[46] C. Tapeinos, E.K. Efthimiadou, N. Boukos, C.A. Charitidis, M. Koklioti, G. Kordas, J. Mater. Chem. B 1 (2013) 194–203.
[47] C. Tapeinos, E.K. Efthimiadou, N. Boukos, C.A. Charitidis, M. Koklioti, G. Kordas, J. Mater. Chem. B 1 (2013) 194–203.
[48] H. Chun Zeng, Curr. Nanosci. 3 (2007) 177–181.
[49] b. Christos Tapeinos, K. Eleni, Efthimiadou, Nikos Boukosa, George Kordas, Colloids Surfaces B Biointerfaces (2016).
[50] M. Heidari Majd, J. Barar, D. Asgari, H. Valizadeh, M.R. Rashidi, V. Kafil, J. Shahbazi, Y. Omidi, Adv. Pharmaceut. Bull. 3 (2013) 189–195.
[51] G. Das, A. Nicastri, M.L. Coluccio, F. Gentile, P. Candeloro, G. Cojoc, C. Liberale, F. De Angelis, E. Di Fabrizio, Microsc. Res. Tech. 73 (2010) 991–995.
[52] T. Mosmann, J. Immunol. Methods 65 (1983) 55–63.
[53] D. Psimadas, H. Oliveira, J. Thevenot, S. Lecommandoux, P. Bouziotis, A.D. Varvarigou, P. Georgoulias, G. Loudos, Pharm. Dev. Technol. 19 (2014) 189–193.
[54] I. Zolle, Springer, (2007).
[55] R. Madru, P. Kjellman, F. Olsson, K. Wingardh, C. Ingvar, F. Stahlberg, J. Olsrud, J. Latt, S. Fredriksson, L. Knutsson, S.E. Strand, J. Nucl. Med. : official publication, Society of Nuclear Medicine 53 (2012) 459–463.
[56] G. Burillo, E. Bucio, E. Arenas, G.P. Lopez, Macromol. Mater. Eng. 292 (2007) 214–219.
[57] T. Mosmann, J. Immunol. Methods 65 (1983) 55–63.
[58] S. Xu, B.Z. Olenyuk, C.T. Okamoto, S.F. Hamm-Alvarez, Adv. Drug Deliv. Rev. 65 (2013) 121–138.
[59] Z. Luo, X. Ding, Y. Hu, S. Wu, Y. Xiang, Y. Zeng, B. Zhang, H. Yan, H. Zhang, L. Zhu, J. Liu, J. Li, K. Cai, Y. Zhao, ACS Nano 7 (2013) 10271–10284.
[60] J. Li, Y. Hu, J. Yang, W. Sun, H. Cai, P. Wei, Y. Sun, G. Zhang, X. Shi, M. Shen, J. Mater. Chem. B 3 (2015) 5720–5730.
[61] C.L. Morton, P.J. Houghton, Nat. Protoc. 2 (2007) 247–250.
[62] T. Kubota, H. Yamaguchi, M. Watanabe, T. Yamamoto, T. Takahara, T. Takeuchi, T. Furukawa, S. Kase, S. Kodaira, K. Ishibiki, M. Kitajima, Surg. Today 23 (1993) 375–377.
[63] Y. Li, H.L. Ho Duc, B. Tyler, T. Williams, M. Tupper, R. Langer, H. Brem, M.J. Cima, J. Control. Release: Off. J. Contr. Release Soc. 106 (2005) 138–145.
[64] N. Voigt, P. Henrich-Noack, S. Kockentiedt, W. Hintz, J. Tomas, B.A. Sabel, J. Nanoparticle Res. 16 (2014).
[65] S. Ning, K. Macleod, R.M. Abra, A.H. Huang, G.M. Hahn, Int. J. Radiat. Oncol. Biol. Phys. 29 (1994) 827–834.